

## Heavy-ion emission from short-pulse laser-plasma interactions with thin foils

N. Sinenian, G. Fiksel, J. A. Frenje, C. G. Freeman, M. J.-E. Manuel et al.

Citation: *Phys. Plasmas* **19**, 093118 (2012); doi: 10.1063/1.4754308

View online: <http://dx.doi.org/10.1063/1.4754308>

View Table of Contents: <http://pop.aip.org/resource/1/PHPAEN/v19/i9>

Published by the [American Institute of Physics](#).

---

### Related Articles

First measurements of laser-accelerated proton induced luminescence

*Phys. Plasmas* **19**, 094501 (2012)

Density and temperature effects on Compton scattering in plasmas

*Phys. Plasmas* **19**, 093115 (2012)

Ultra-relativistic ion acceleration in the laser-plasma interactions

*Phys. Plasmas* **19**, 093109 (2012)

Effect of target composition on proton acceleration in ultraintense laser-thin foil interaction

*Phys. Plasmas* **19**, 093108 (2012)

Generation of high-energy (>15 MeV) neutrons using short pulse high intensity lasers

*Phys. Plasmas* **19**, 093106 (2012)

---

### Additional information on Phys. Plasmas

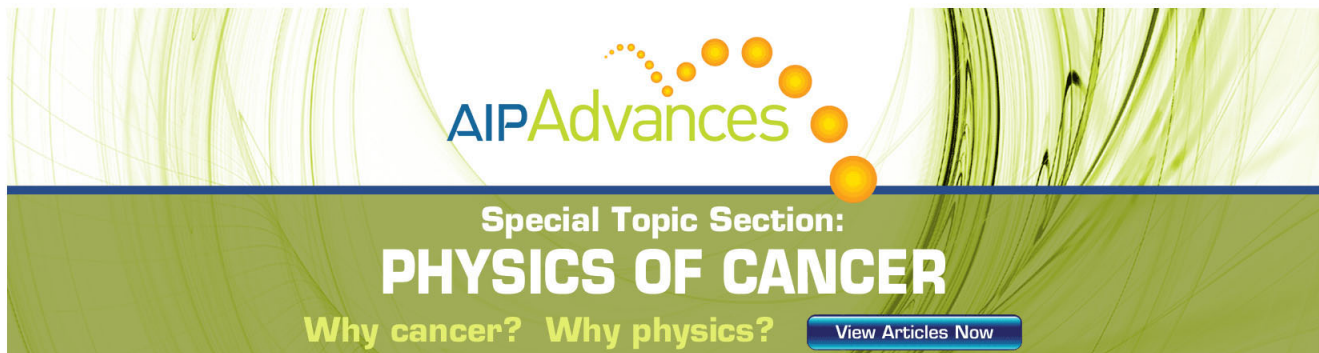
Journal Homepage: <http://pop.aip.org/>

Journal Information: [http://pop.aip.org/about/about\\_the\\_journal](http://pop.aip.org/about/about_the_journal)

Top downloads: [http://pop.aip.org/features/most\\_downloaded](http://pop.aip.org/features/most_downloaded)

Information for Authors: <http://pop.aip.org/authors>

## ADVERTISEMENT



**AIP Advances**

Special Topic Section:  
**PHYSICS OF CANCER**

Why cancer? Why physics? [View Articles Now](#)

# Heavy-ion emission from short-pulse laser-plasma interactions with thin foils

N. Sinenian,<sup>1,a)</sup> G. Fiksel,<sup>2</sup> J. A. Frenje,<sup>1</sup> C. G. Freeman,<sup>3</sup> M. J.-E. Manuel,<sup>1</sup> D. T. Casey,<sup>1</sup> P. M. Nilson,<sup>2</sup> C. Stoeckl,<sup>2</sup> W. Theobald,<sup>2</sup> D. D. Meyerhofer,<sup>2,b)</sup> and R. D. Petrasso<sup>1</sup>

<sup>1</sup>Plasma Science and Fusion Center, Massachusetts Institute of Technology, Cambridge, Massachusetts 02139, USA

<sup>2</sup>Laboratory for Laser Energetics, Rochester, New York 14623, USA

<sup>3</sup>State University of New York at Geneseo, Geneseo, New York 14454, USA

(Received 10 February 2012; accepted 7 September 2012; published online 26 September 2012)

A Thomson parabola ion spectrometer, implemented on the Laboratory for Laser Energetics Multi-Terawatt laser facility, has been used to study heavy-ion acceleration from ultra-intense laser-plasma interactions. These studies were conducted using 20  $\mu\text{m}$ -thick flat foil targets with on-target intensities of  $4\text{--}5 \times 10^{19} \text{ W}\cdot\text{cm}^{-2}$ . Several charge states of energetic heavy ions were accelerated from the rear of Al and Cu foils in the presence of hydrocarbon contaminants. In contrast to previous work, we show that the mean and maximum energies of each heavy-ion species scale linearly with only the charge of the ion, and not the charge-to-mass ratio, implying that the space-charge is not readily depleted as ions expand. It has been shown previously and observed here that the maximum heavy-ion energies are lower than that of protons, though a fundamental explanation for this discrepancy has not been provided. We show how a two-temperature electron distribution, observed in these experiments, explains these observations.

© 2012 American Institute of Physics. [<http://dx.doi.org/10.1063/1.4754308>]

## I. INTRODUCTION

Acceleration of fast ions generated by high-intensity laser-plasma interactions (LPI) is an important topic due to its applications in medicine, high-energy-density physics (HEDP)<sup>1</sup> and table-top particle accelerators. Medical applications include generation of protons and energetic carbon ions for cancer therapy.<sup>2,3</sup> HEDP applications involve the development of high-energy proton backlighters for high-resolution imaging studies (e.g., field structures in inertial confinement fusion (ICF) implosions).<sup>4–7</sup> A better and fundamental understanding of the underlying physics in generating and accelerating ions is important for optimizing advanced fusion concepts, such as ion fast-ignition.<sup>8</sup>

Over the last decade, a number of experimental studies have been conducted on proton acceleration from thin foils. The effects of target parameters (geometry and materials) and laser parameters (pulse duration, contrast, and intensity) on proton acceleration have been extensively studied and compared to theory.<sup>9–13</sup> The acceleration of heavy-ions has also been observed and enhanced by removing hydrocarbon contaminants.<sup>14–17</sup> This enhancement has been attributed to the fact that protons and lighter ions have a lower charge-to-mass ratio and are therefore preferentially accelerated, after which the accelerating space-charge is depleted.

In contrast to previous work, we demonstrate here that the mean and maximum energies of heavy ions scale with only the charge state and not the charge-to-mass ratio for several ion species. Consistent with past work, it is observed here that the maximum heavy-ion energies are lower than

that of contaminant protons. We have observed the signature of a two temperature electron distribution and discuss how this distribution explains the observed heavy-ion scalings in the presence of protons. Current ion-expansion models show excellent agreement with proton data but do not incorporate multi-species heavy ions. The data presented here are essential for any modeling of multi-species heavy-ion acceleration in the presence of a two-temperature electron distribution. Although such electron distributions have been previously predicted by simulations<sup>18</sup> and observed using electron diagnostic techniques,<sup>19</sup> its implications on ion acceleration have not been explicitly observed.

The heavy-ion measurements were taken at the Multi-Terawatt (MTW) laser facility<sup>20</sup> at the Laboratory for Laser Energetics (LLE). The MTW laser served as a prototype front-end for the OMEGA-EP<sup>21</sup> ultra-intense laser, and continues to function as a stand-alone laser, capable of delivering on-target energies as high as 10 J of IR light (1053 nm) in 1 ps. On-target intensities as high as  $5 \times 10^{19} \text{ W}\cdot\text{cm}^{-2}$  with a contrast of  $10^8$  are possible at best focus, where 50% of the laser energy is focused to a 5  $\mu\text{m}$  diameter spot. In addition to being a platform for developing diagnostics for OMEGA-EP<sup>22</sup> and damage testing of optics, the MTW is being used for studies of LPI in the context of backlighter development and basic science. A Thomson parabola ion spectrometer (TPIS),<sup>23–27</sup> previously designed, constructed and implemented on the MTW, was used for measurements of charged particle energy spectra.

This paper is organized as follows: We first present an overview of the TPIS and simulations of its response to heavy-ions (Sec. II). In Sec. III, heavy-ion experiments and results are presented, followed by a discussion of the physics and implications of these results (in Sec. IV). Section V

<sup>a)</sup>nareg@psfc.mit.edu.

<sup>b)</sup>Also at Department of Mechanical Engineering and Physics, University of Rochester, New York 14623, USA.

concludes by discussing future measurements and some features of the detection scheme which are still being developed.

## II. THE TPIS AND RESPONSE TO HEAVY IONS

As shown in Fig. 1, the main components comprising the TPIS diagnostic<sup>27</sup> are a circular aperture, a permanent magnet (5.4 kg), electrostatic deflector plates (80 kV max) and a detector assembly consisting of CR-39 and an image plate. The detector pocket can accommodate either a 10 cm × 10 cm, 1.5 mm thick piece of CR-39<sup>28,29</sup> or a Fuji TR IP,<sup>30</sup> or a stacked detector assembly consisting of both. The CR-39, which is a clear plastic nuclear track detector with the advantage of being immune to EMP and x-rays, is used extensively at the OMEGA laser facility and recently at the NIF.<sup>31–33</sup> It is capable of detecting all heavy ions and protons with energies up to about 8 MeV with 100% efficiency; at higher energies the efficiency decreases with the stopping power of protons in CR-39.<sup>32</sup> The Fuji IPs are capable of detecting some high-Z ions and protons with energies up to at least 20 MeV, though the sensitivity is a strong function of energy. An absolute calibration of the IP response to protons was recently conducted at SUNY Geneseo for proton energies in the range of 0.6–3.4 MeV.<sup>27</sup> As the Fuji TR lacks a protective layer of Mylar found on other IPs, carbon ions can be detected as well. IPs are ideal for measurements of energetic protons, whereas CR-39 is essential for detection of high-Z ions.

The first consideration for heavy-ion measurements using CR-39 in the TPIS is the acceptable range of ion fluences on the CR-39. This range is set by the intrinsic noise floor at the low end and saturation (track overlap) of the detector at the high end. The on-detector fluence requirements are a minimum of about  $10^4$  proton tracks/cm<sup>2</sup> for good statistics relative to the background intrinsic noise, and no more than proton  $10^6$  tracks/cm<sup>2</sup> to avoid track overlap.<sup>32</sup> After accounting for the standard 400 μm aperture and 50 cm target-to-aperture distance, this requirement translates to an

acceptable fluence range of  $10–10^3$  ions/μsr. This number is a conservative estimate because (1) dispersion due to the fields smears out the same number of ions over a larger detection area (2) the details of the spectral shape (e.g., peak location or width) will change this limit, as a broader spectrum in energy space corresponds to a broader spread across the detector for the same number of ions, and (3) heavier ions will leave larger tracks on the CR-39 and for those ions this number becomes less conservative. The etch time of CR-39 may be adjusted on a per-shot basis to accommodate a wide range of ion fluences, effectively increasing the dynamic range of the detector.

A second consideration for heavy-ion measurement with the TPIS is the instrument response to these ions. The deflection of ions in the TPIS due to uniform magnetic and electric fields scale as  $\sim Zk_B/(E_p A)^{1/2}$  and  $\sim Z \cdot k_E/E_p$ , respectively.<sup>27</sup> Here,  $Z$  is the ion charge state,  $A$  is the atomic number and  $E_p$  is the energy of the particle. The constants  $k_B$  and  $k_E$  depend on geometric factors and are fixed. The deflection of ions due to these fields results in a family of parabolas at the detector plane, where the slope of each parabola is given by  $\alpha \equiv A/Z \cdot k_E/k_B^2$ . Thus,  $\alpha$  defines the slope of the parabolic distribution of particles, with a given mass-to-charge ratio ( $A/Z$ ), at the detector plane. Each position along that parabola corresponds to a unique velocity, which can be converted to an energy. Note that once the species has been identified by its slope, the magnetic (or electric) deflection is sufficient to determine the energy of the particle. For accurate identification of the particle species and precise determination of ion energies, it is important to verify that these scalings hold for a range of heavy-ions.

The initial TPIS calibration was obtained through experiments at SUNY Geneseo.<sup>27</sup> These experiments were performed with 0.6–3.4 MeV protons to obtain the magnet energy calibration, while additional experiments using 0.8–3.4 MeV protons were conducted to calibrate the line-integrated electric field strength. Although these calibrations are in excellent agreement with the nominal scalings, it is not clear that they may be extrapolated and applied to more energetic ions with a large mass-to-charge ratio, such as C, Cu, or Al. These heavier ions, which traverse a different part of the magnet and electrodes, may experience non-uniformities and fringe fields that lighter ions do not. For densely packed parabolas (e.g., lower operating voltages or higher-Z targets) a calibration accurate to within just a few percent is required to correctly identify the particle species and charge state. A charged-particle ray-tracing code was developed and used to compute the trajectories through the field maps for a range of ions, charge states and energies. The magnetic field map was supplied by Dexter Magnetic Technologies Inc.,<sup>34</sup> and the electric field map was generated by a finite-element method (FEM). The FEM approach used detailed models of the electrodes including the Ultem<sup>TM</sup> dielectric ( $\kappa \approx 3$ ) to which they are affixed, as well as the instrument housing. The potentials on these surfaces were solved for at all locations using the appropriate boundary conditions. The electric fields were computed using a finite-difference of the three-dimensional potential map using a fine grid.

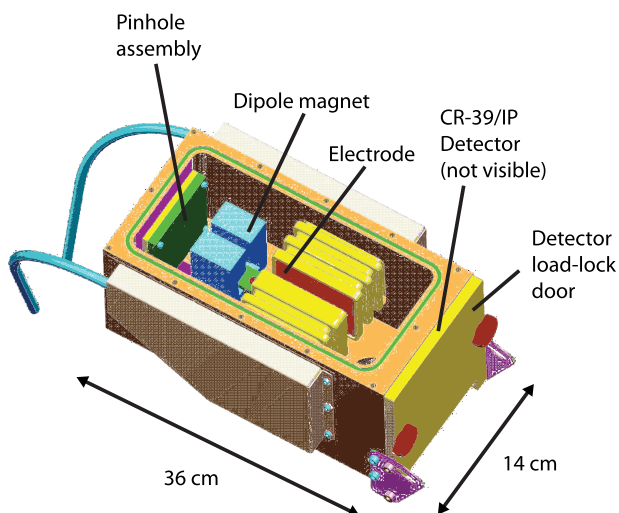


FIG. 1. Cut-away view of the TPIS, showing the dipole magnet (blue) and electrodes (red); the pinhole is on the left and the detector pocket on the right.

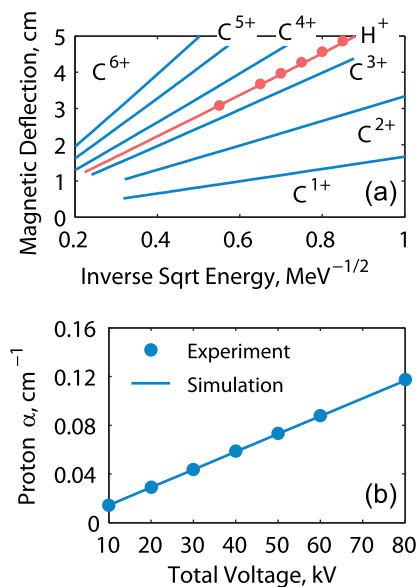


FIG. 2. (a) Simulated magnetic deflection as a function of inverse energy for protons and carbon ions; the field strength was scaled by 3% to match the SUNY Geneseo calibration experiments that used 0.6–3.4 MeV protons (red circles). (b) Simulated (MIT) and measured (SUNY Geneseo) parabola slopes ( $\alpha$ ) for 1.07 MeV protons. Simulations were benchmarked against Geneseo proton calibrations and extrapolated for heavy-ions, as shown.

The simulated results for the magnet energy scaling of protons and carbon ions are shown in Fig. 2(a). The magnetic field map had to be scaled in strength by approximately 3% to match the experimentally determined energy scaling.<sup>27</sup> This systematic difference may be attributed to the position accuracy of the field map (since there is likely to be a systematic discrepancy between the simulated and constructed magnet assembly), as well as small offsets in the alignment of the magnet relative to the housing of the as-built TPIS. The magnetic energy calibration has been combined with simulations of the electrostatic deflection of protons in the TPIS to obtain a derived calibration for  $\alpha$  as a function of electrode voltage. This is illustrated in Fig. 2(b) alongside the SUNY Geneseo calibrations.<sup>27</sup>

### III. EXPERIMENTS AND RESULTS

Initial TPIS experiments on the MTW laser were conducted using  $500 \mu\text{m} \times 500 \mu\text{m}$  square aluminum and copper foil targets with a thickness of  $20 \mu\text{m}$ , as shown in Fig. 3. The foils were irradiated with a laser energy of about 8.5 J, delivered in 1 ps. The full width at half maximum (FWHM) focal spot size was  $5 \mu\text{m}$  in diameter, resulting in on-target intensities between  $4\text{--}5 \times 10^{19} \text{ W}\cdot\text{cm}^{-2}$ . The foils were oriented in such way that the TPIS measured energetic protons accelerated normal to the rear of the foils.

Resulting data from the CR-39, after a 20 min etch in a 6N solution of NaOH held at  $80^\circ\text{C}$ , is shown in Fig. 4(a) in the form of a 2D histogram of track density, mapped to colors by a lookup table to generate an artificial image. Sample IP data are shown in Fig. 4(b). Several charge states of carbon and aluminum ions are present in the CR-39 data, while protons are not observed due to a short etch time. Longer etch

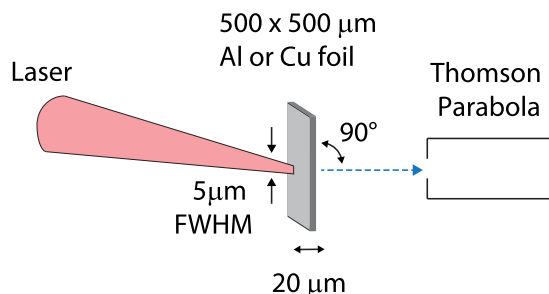


FIG. 3. Setup of the experiments presented in this paper. The TPIS measured energetic protons accelerated normal to the rear of the flat-foil targets. The laser had a time constant of 1 ps and a contrast of  $10^8$ .

times could not be applied to the CR-39, as that would have caused significant overlap (saturation) of the heavy-ion tracks. From the parabolas shown in Figs. 4(a) and 4(b), the particle distribution as a function of  $\alpha$  can be determined by establishing the parabola boundaries and then binning the number of track counts along that parabola. One example of an  $N(\alpha)$  distribution is shown in Fig. 5, which spans the entire range of possible  $\alpha$ -values for the Al target. Several strong lines are present as well as many weaker ones; the expanded inset of Fig. 5 shows a view of the  $\alpha$ -spectrum and highlights the weaker lines. These background-subtracted distributions are used to identify the ion species by the using the  $\alpha$ -value associated with the center of a peak. Once the  $N(\alpha)$  distribution has been established, the number of tracks as a function of energy can be determined from the magnetic displacement (horizontal direction) by using the magnet energy scaling.

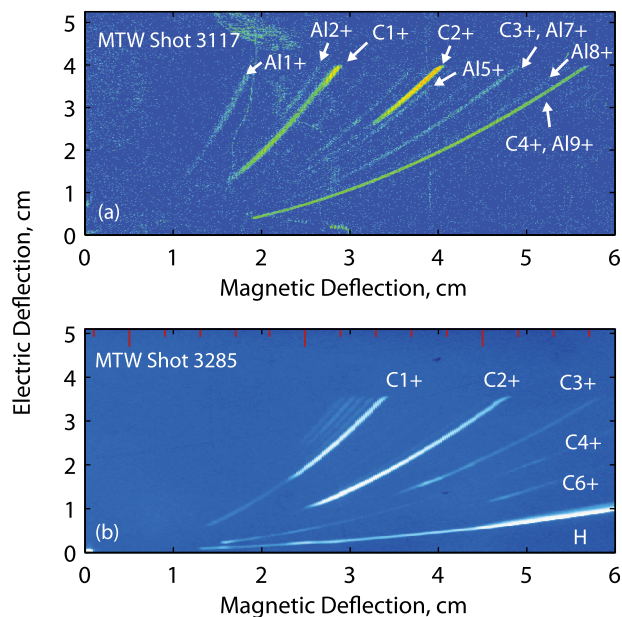


FIG. 4. (a) CR-39 data from MTW shot 3117 showing various heavy-ion parabolas. Lighter regions indicate higher track density; the lookup table was artificially saturated to enhance the visual appearance of parabolas. Note the localized areas of noise on the detector (e.g., bottom center of image). The TPIS was operated at 30 kV for this shot. (b) IP data for MTW shot 3285, showing carbon and proton parabolas. The TPIS was operated at voltage of 20 kV for this shot.

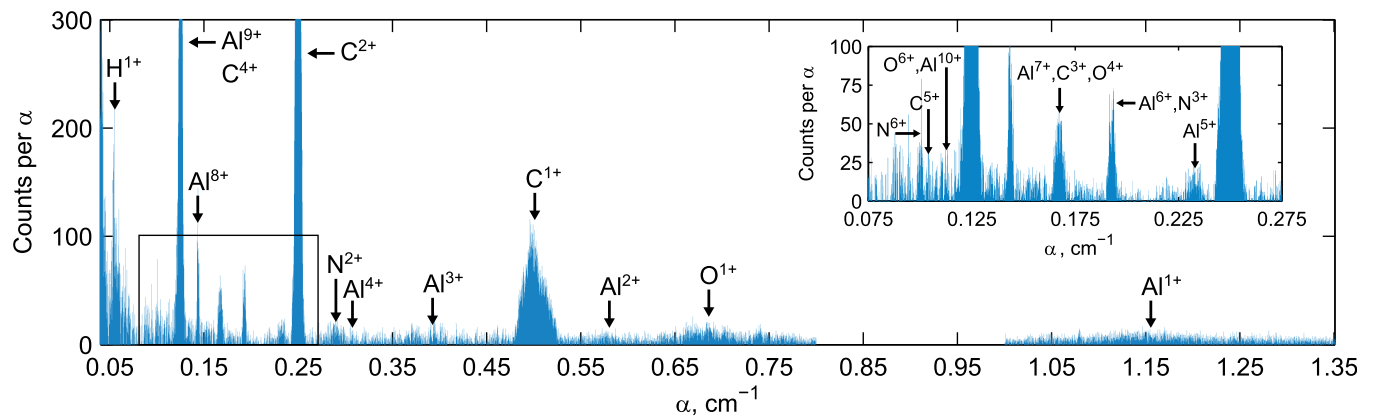


FIG. 5. Histogram of the number of tracks recorded on the CR-39, binned in  $\alpha$ -space, for a  $500 \times 500 \times 20 \mu\text{m}$  Al flat foil irradiated with a laser intensity of  $5 \times 10^{19} \text{ W/cm}^2$ . An expanded view of the boxed region is shown as an inset, with several more weaker lines and a few overlapping parabolas. All labeled ions were separable with the exception of  $\text{Al}^{9+}$  and  $\text{C}^{4+}$ . Some localized noise has also been identified and removed (by correlating the  $N(\alpha)$  histogram with  $N(x,y)$  images.)

Fig. 5 shows that the TPIS, operating at an electric field of  $15 \text{ kV/cm}$  with an aperture of  $400 \mu\text{m}$ , was not able to differentiate some of the high-Z ions (e.g.,  $\text{C}^{5+}$  and  $\text{N}^{6+}$ ). To resolve this a smaller aperture should be used to decrease the parabolic line broadening. Alternatively, a stronger electric field (e.g.,  $40 \text{ kV/cm}$ ) can be used if the signal is weak. Magnetic focusing increases with increasing charge-to-mass ratios, since these ions undergo greater magnetic deflection, resulting in broader lines in  $\alpha$ -space.

Since each parabola is divided into constant energy bins with each bin spanning a small but finite distance along the spatial direction of magnetic displacement, the background level is determined from just above and below the parabola. The background is interpolated through the parabola in the direction of electric displacement. Figures 6 and 7 show the results from this background subtraction analysis for several ion species from aluminum and copper flat foils, respectively. Figure 8 shows proton energy spectra measured by image plates for four MTW shots of comparable laser intensities and targets (3280, 3281, 3285, 3286). Shown in these background-subtracted spectra are the error bars arising from the statistical uncertainty (95% confidence limit) of the measurement. The highest proton energies measured by the IP agree with theoretical predictions<sup>9,11</sup> for these targets and laser intensities. Predictions for aluminum or carbon ions at different charge states are not available at this time; empirical scalings are presented in the following section.

The heavy-ion spectra acquired in these experiments have been used to study the underlying physics. The spectra shown in Figs. 6 and 7 from aluminum and copper targets, respectively, illustrate a strong signal of certain ions and charge states over others. Note that the spectra from the aluminum target exhibits strong  $\text{C}^{1+}$  and  $\text{C}^{2+}$  lines while the data from the copper target does not. It has been previously shown that ultra-intense laser beams incident on flat foils preferentially accelerate protons and hydrocarbons.<sup>16</sup> To increase the heavy-ion energy for medical and ion fast-ignition applications, techniques have been developed to mitigate energy coupling to contaminant ions (e.g. protons) using cleaning techniques and specific target materials.<sup>16</sup> In experiments described here, no effort was made to remove

these hydrocarbon contaminants; the difference illustrated here in the acceleration of carbon ions between aluminum and copper is likely due to the variation of contaminant levels between targets.

Despite this difference between targets, there are trends in the mean and maximum ion energy of these ions, as illustrated in Fig. 9. The mean energies were determined by integrating (and normalizing) the spectra of Figs. 6 and 7 along with the proton spectra of Fig. 8. The precision of these measurements is limited by three factors. First, the energy resolution of the TPIS, when run with a  $400 \mu\text{m}$  aperture, has a worst-case uncertainty of approximately 6% for 20 MeV proton equivalent energies; this can be as low as 1% for

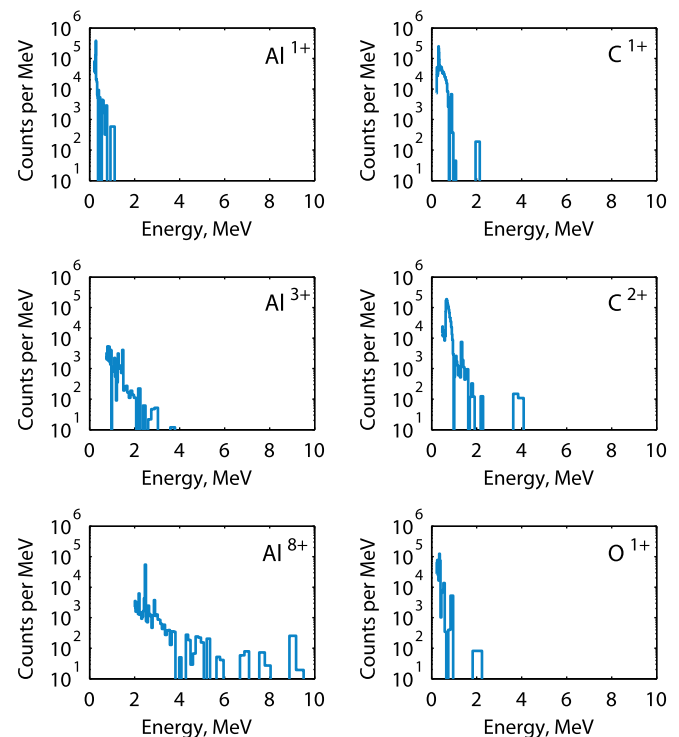


FIG. 6. Sample heavy-ion energy spectra for MTW Shot 3117, obtained using CR-39. Target was a  $500 \times 500 \times 20 \mu\text{m}$  aluminum foil, irradiated with a laser intensity of  $5 \times 10^{19} \text{ W/cm}^2$ .

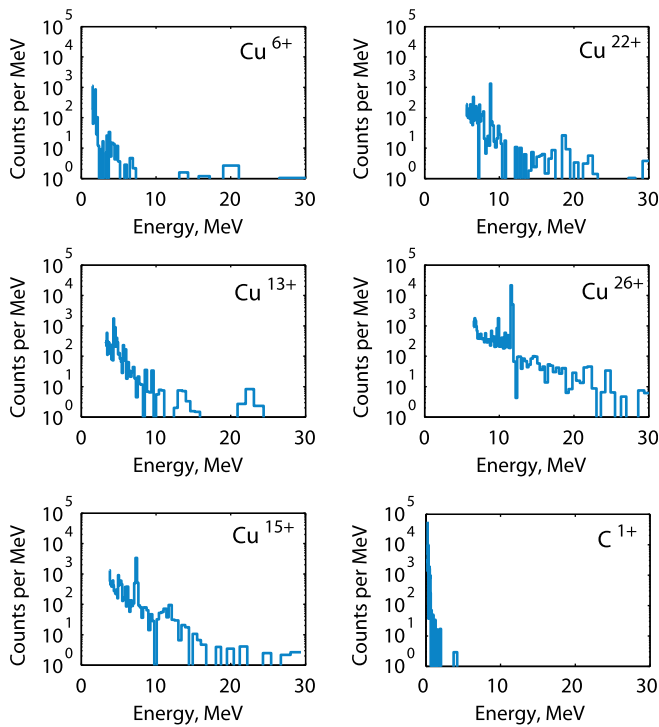


FIG. 7. Sample heavy-ion energy spectra for MTW Shot 3118, obtained using CR-39. Target was a  $500 \times 500 \times 20 \mu\text{m}$  copper foil, irradiated with a laser intensity of  $4 \times 10^{19} \text{W}\cdot\text{cm}^{-2}$ .

300 keV protons. Second, proper alignment of CR-39 during a microscope scan is limited to offsets as high as  $200 \mu\text{m}$  in the magnet dispersion direction, resulting in uncertainties as high as 3.8%. The third contribution is the uncertainty arising from counting statistics, which in these data were no higher than a few percent. These three uncorrelated quantities were used to compute the error bars (within 95% confidence limits) shown in Fig. 9. These upper-bound estimates neglect the effect of the electric field on resolution; they are thus conservative estimates. The estimates of maximum

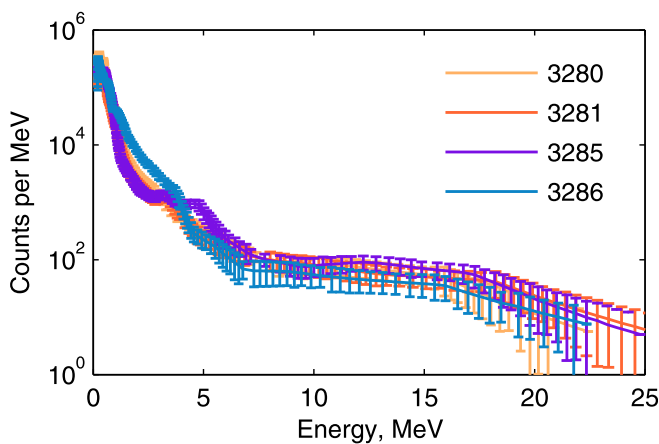


FIG. 8. Proton energy spectra measured on MTW Shots 3280, 3281, 3285, and 3286 using Fuji Type TR IPs, demonstrating good shot-to-shot repeatability. Targets were  $500 \times 500 \times 20 \mu\text{m}$  Cu flat foils, irradiated with laser intensities of approx.  $4 \times 10^{19} \text{W}\cdot\text{cm}^{-2}$ . Shown are statistical error bars (95% confidence limits) for each of the spectra. The maximum energies are not well-defined. They were taken to be the knee of the spectra between 15 and 20 MeV where the statistics are poor.

energies shown in Fig. 9 include a systematic observational bias of about 20% (not shown in the error bars) arising from the inability to visually discern an exact cutoff; this is evident in the spectra shown in Figs. 6 and 7. For the proton energy spectra (Fig. 8) the cutoff is also difficult to determine. It was taken to be the knee of the spectra between 15 and 20 MeV. There are fewer than 200 protons above this defined cutoff, which is significantly lower than the number of protons under either of the two slopes in the spectra.

It has been suggested that protons, being lighter, are preferentially accelerated over heavier ions and thus will deplete the space-charge initially setup by hot escaping electrons.<sup>10</sup> This would lead to a scaling of the bulk ion energy with the charge-to-mass ratio rather than the charge, since lighter ions with higher charge states would be accelerated first, lowering the space-charge field for subsequent ions. These data, which include several species of aluminum, copper, carbon, oxygen, and nitrogen ions (Fig. 9), show

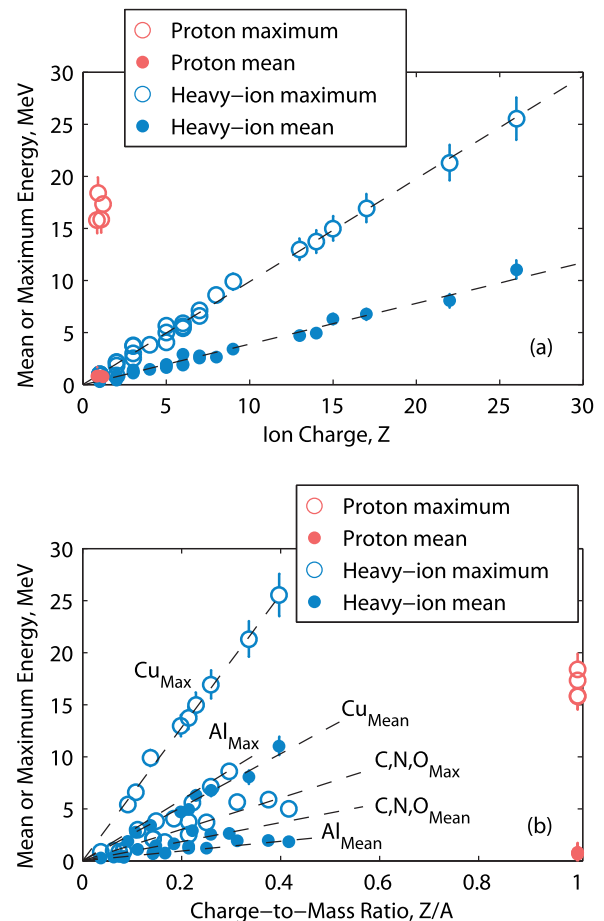


FIG. 9. (a) Mean ion energy and maximum energy vs. charge for protons and heavy ions. The proton were obtained from image plates over four shots of comparable intensity (3280, 3281, 3285, 3286); heavy ions shown here include several charge states of aluminum, copper, carbon, nitrogen and oxygen acquired over two flat-foil shots (3117 and 3118). Note the linear scaling of maximum energies among the heavy ions; the proton maximum energies are significantly higher and do not fit this trend. Note the maximum ion energies are subject to a 20% systematic observational bias (the shown error bars represent only the statistical uncertainty). (b) Mean and max ion energies vs. charge-to-mass ratio ( $Z/A$ ) show linear scaling with charge for a fixed mass.

excellent scaling between mean energy and charge rather than with charge-to-mass ratio. A chi-square analysis shows that the mean energy for all ions is best described by the linear fit

$$E_{Mean} = 0.38 \times Z - 0.07, \quad (1)$$

with  $\chi^2 = 0.98$ . The scaling suggests that the sheath potential does not deplete over the acceleration phase of these ions. The maximum energies show similar scaling for the *heavy* ions. For these ions, a chi-square analysis shows that maximum energy scales as

$$E_{Max.} = 0.99 \times Z - 0.09, \quad (2)$$

with  $\chi^2 = 0.99$ . The maximum energies of heavy ions are significantly higher than the mean, reflecting the fact that the bulk of the ions experience much lower sheath fields. The maximum energies of protons are significantly higher than those of the heavy ions and do not fit the same linear trend.

#### IV. DISCUSSION

The observed discrepancy in maximum energies between protons and heavy-ions may be explained by the presence of a two-temperature electron distribution. Simulations<sup>18,35</sup> and Cu K- $\alpha$  line measurements<sup>19</sup> have shown the presence of a two-temperature electron distribution for comparable targets and laser intensities, and the two slopes in the proton spectra of Fig. 8 suggest that a two-temperature distribution is prevalent in these experiments.

In the two-temperature theoretical framework,<sup>18,35</sup> the two distributions are characterized by a hot ( $T_h$ ) and a cold ( $T_c$ ) temperature, with respective number densities ( $n_h$  and  $n_c$ ) and pressures ( $p_h$  and  $p_c$ ). As the laser propagates through the underdense pre-plasma, a small fraction of electrons are directly heated by the laser. For a short-pulse interaction these electrons do not have time to reach thermal equilibrium with the bulk electrons. Thus, a two-temperature electron distribution with  $n_h \ll n_c$  and  $\nabla p_h/n_h \gg \nabla p_c/n_c$  is probable. The hot component will generate stronger sheath fields than the cold component (because the sheath fields  $\propto \nabla p/n$ ). However, since  $n_h \ll n_c$ , the charge separation is weaker for the hot component than for the cold component. Given these limits, the hot component will accelerate a small fraction of the protons to higher maximum energies; these protons will then quickly shield the sheath fields associated with the hot component since the charge separation is weak by assumption. Heavier ions and the bulk of the slower protons will experience fields generated by the colder component, and therefore have lower maximum energies. Furthermore, if the cold component has enough charge separation, the heavy-ion mean and maximum energies will scale as a function of  $Z$ , and not  $Z/A$ .

In these models, the maximum energy a proton will reach in connection with the cold electron ( $T_c$ ) component is<sup>18</sup>

$$E_{Max.,C} = 2\sqrt{2} \frac{eE_L}{m_e c \omega_0} \times 511 \text{ keV}, \quad (3)$$

where  $E_L$  is the laser electric field,  $m_e$  is the electron mass, and  $\omega_0$  is the laser frequency. For these experiments, we estimate  $E_{Max.,C} \approx 8 \text{ MeV}$ , which nearly coincides with the knee in the measured proton spectra at  $\sim 7 \text{ MeV}$ , as shown in Fig. 8. In these experiments, protons with energies greater than 7 MeV are accelerated due to a hot-electron component.

Simulations<sup>35</sup> have shown that for  $n_c/n_h \approx 200$  and initial temperature ratios of  $T_h/T_c \approx 900$ , the hot-electron temperature falls on a time-scale much faster than the cold component.<sup>35</sup> In addition, 3D PIC simulations<sup>18</sup> have shown that for  $n_c/n_h \approx 100$  and  $T_h/T_c \approx 50$ , a smaller population of energetic ions are accelerated from the rear of the target in association with the hot component while slower ions are accelerated from the front of the target (towards the rear) due to the cold component. In these experiments, we estimate  $n_c/n_h \sim 200$  by integrating the left and right sides of the dual-slope proton spectra of Fig. 8.  $T_h/T_c \sim 50$  is estimated from the two slopes of the proton spectra.

These experiments are in a regime comparable to the simulations. The experimental results are consistent with a simulated hot-electron component that drives fewer energetic protons to high energies for a short period of time and then decays away quickly, leaving a cold component with strong charge separation to accelerate heavy ions for an extended duration.

These data have important implications for heavy-ion fast-ignition and for cancer therapy because they suggest that acceleration of a specific ion species (and charge state) is not easily controlled. Even if the acceleration of contaminants or undesired elements are suppressed by novel methods, coupling of energy into a pure beam of a pre-specified  $Z/A$  is not trivial. As previously mentioned, no effort was made in these experiments to suppress the acceleration of protons or hydrocarbons. It has been demonstrated in the past that resistive heating of targets reduces the number of unwanted accelerated hydrocarbons and that by coating the rear of the target one may preferentially accelerate ions of a particular element (but not charge state).<sup>15</sup> However, even for the case of heated targets, observations showed preferential acceleration and energy coupling to ion species with the highest charge-to-mass ratio. Furthermore, those experiments were used to infer two electric fields: the first was a strong, short-lived field associated with the acceleration of ions with the highest charge-to-mass ratio, and the second was a weaker field with a longer timescale that drove all other ions.<sup>15</sup> We make the connection between these observations and those presented here with the presence of a two-temperature electron distribution that follows the density and temperature ordering as described.

The results have an adverse impact in the context of the aforementioned applications. For cancer therapy, an ion with a given energy will have less penetrating power (and damage more surface tissue) when its charge state is higher. For ion fast-ignition applications, a higher charge state suggests more blooming of the generated ion beam, less localized power deposition, and higher ignition requirements. It is therefore desirable to increase the energy and number of ions without increasing the charge number.

## V. CONCLUDING REMARKS

A TPIS, previously implemented at the MTW laser facility, has been used to study the underlying mechanisms of heavy-ion acceleration. In initial experiments utilizing flat-foil targets at on-target intensities of  $4\text{--}5 \times 10^{19} \text{ W}\cdot\text{cm}^{-2}$ , energetic protons (15–18 MeV max) as well as several energetic heavy-ions, including species of carbon, aluminum, copper, nitrogen, and oxygen were observed. Empirical scalings of the mean and maximum energies of heavy-ions were determined.

In contrast to previous work, it has been shown here that the mean energies of heavy-ions scale linearly with only the charge of the ion, and not the charge-to-mass ratio, implying that the space-charge is not readily depleted as ions expand. The discrepancy in maximum energies between protons and heavy-ions, and the scaling of the heavy-ion energies, is explained by a two-temperature electron distribution where the hot component has weak charge separation.

Future experiments will study the dependence of the heavy-ion scalings on intensity and further probe the regime of two-temperature electron distributions. The detection scheme will also be improved by (1) minimizing loss of proton spectra associated with stopping of protons in CR-39 when IPs and CR-39 are used simultaneously and (2) better calibration of the IP response to protons in the high-energy range; note that while empirical calibrations have been undertaken for 1–20 MeV protons,<sup>36</sup> there is no physical explanation for the resulting calibration.

## ACKNOWLEDGMENTS

The authors express their thanks to the engineering staff at LLE for their support in the development and calibration of this diagnostic. We also thank Chad Mileham and Ildar Begishev, whose expertise was essential in acquiring experimental data at the MTW Facility. This work was done in part for the author's Ph.D. thesis, and was supported in part by NLUF (DOE Award No. DE-NA0000877), FSC Rochester Sub Award PO No. 415023-G), US DOE (Grant No. DE-FG03-03SF22691), LLE (No. 412160-001G), LLNL (No. B504974), and GA under DOE (DE-AC52-06NA27279).

<sup>1</sup>N. R. C. Committee on High Energy Density Plasma Physics, Plasma Science Committee, *Frontiers in High Energy Density Physics: The X-Games of Contemporary Science* (The National Academies Press, 2003).

<sup>2</sup>C. Ma, I. Veltchev, E. Fourkal, J. Li, W. Luo, J. Fan, T. Lin, and A. Pollock, *Laser Phys.* **16**, 639 (2006).

<sup>3</sup>U. Linz and J. Alonso, *Phys. Rev. ST Accel. Beams* **10**, 094801 (2007).

<sup>4</sup>J. A. Stamper, K. Papadopoulos, R. N. Sudan, S. O. Dean, E. A. McLean, and J. M. Dawson, *Phys. Rev. Lett.* **26**, 1012 (1971).

<sup>5</sup>C. K. Li, F. H. Séguin, J. A. Frenje, J. R. Rygg, R. D. Petrasso, R. P. J. Town, P. A. Amendt, S. P. Hatchett, O. L. Landen, A. J. Mackinnon, P. K. Patel, V. A. Smalyuk, T. C. Sangster, and J. P. Knauer, *Phys. Rev. Lett.* **97**, 135003 (2006).

<sup>6</sup>C. K. Li, F. H. Séguin, J. A. Frenje, M. Rosenberg, R. D. Petrasso, P. A. Amendt, J. A. Koch, O. L. Landen, H. S. Park, H. F. Robey, R. P. J. Town, A. Casner, F. Philippe, R. Betti, J. P. Knauer, D. D. Meyerhofer, C. A. Back, J. D. Kilkenny, and A. Nikroo, *Science* **327**, 1231 (2010).

<sup>7</sup>J. R. Rygg, F. H. Séguin, C. K. Li, J. A. Frenje, M. J.-E. Manuel, R. D. Petrasso, R. Betti, J. A. Delettrez, O. V. Gotchev, J. P. Knauer, D. D.

Meyerhofer, F. J. Marshall, C. Stoeckl, and W. Theobald, *Science* **319**, 1223 (2008).

<sup>8</sup>M. Roth, T. E. Cowan, M. H. Key, S. P. Hatchett, C. Brown, W. Fountain, J. Johnson, D. M. Pennington, R. A. Snavely, S. C. Wilks, K. Yasuike, H. Ruhl, F. Pegoraro, S. V. Bulanov, E. M. Campbell, M. D. Perry, and H. Powell, *Phys. Rev. Lett.* **86**, 436 (2001).

<sup>9</sup>J. Fuchs, P. Antici, E. d'Humieres, E. Lefebvre, M. Borghesi, E. Brambrink, C. A. Cecchetti, M. Kaluza, V. Malka, M. Manclossi, S. Meyroneinc, P. Mora, J. Schreiber, T. Toncian, H. Pepin, and P. Audebert, *Nat. Phys.* **2**, 48 (2006).

<sup>10</sup>P. McKenna, F. Lindau, O. Lundh, D. Neely, A. Persson, and C.-G. Wahlstrom, *Philos. Trans. R. Soc. London* **364**, 711 (2006).

<sup>11</sup>L. Robson, P. T. Simpson, R. J. Clarke, K. W. D. Ledingham, F. Lindau, O. Lundh, T. McCanny, P. Mora, D. Neely, C. G. Wahlstrom, M. Zepf, and P. McKenna, *Nat. Phys.* **3**, 58 (2007).

<sup>12</sup>S. S. Bulanov, A. Brantov, V. Y. Bychenkov, V. Chvykov, G. Kalinchenko, T. Matsuoka, P. Rousseau, S. Reed, V. Yanovsky, D. W. Litzenberg, K. Krushelnick, and A. Maksimchuk, *Phys. Rev. E* **78**, 026412 (2008).

<sup>13</sup>K. A. Flippo, E. d'Humieres, S. A. Gaillard, J. Rassuchine, D. C. Gautier, M. Schollmeier, F. Nurnberg, J. L. Kline, J. Adams, B. Albright, M. Bakeman, K. Harres, R. P. Johnson, G. Korgan, S. Letzring, S. Malekos, N. Renard-LeGalloudec, Y. Sentoku, T. Shimada, M. Roth, T. E. Cowan, J. C. Fernandez, and B. M. Hegelich, *Phys. Plasmas* **15**, 056709 (2008).

<sup>14</sup>E. L. Clark, K. Krushelnick, M. Zepf, F. N. Beg, M. Tatarakis, A. Machacek, M. I. K. Santala, I. Watts, P. A. Norreys, and A. E. Dangor, *Phys. Rev. Lett.* **85**, 1654 (2000).

<sup>15</sup>M. Hegelich, S. Karsch, G. Pretzler, D. Habs, K. Witte, W. Guenther, M. Allen, A. Blazevic, J. Fuchs, J. C. Gauthier, M. Geissel, P. Audebert, T. Cowan, and M. Roth, *Phys. Rev. Lett.* **89**, 085002 (2002).

<sup>16</sup>B. M. Hegelich, B. Albright, P. Audebert, A. Blazevic, E. Brambrink, J. Cobble, T. Cowan, J. Fuchs, J. C. Gauthier, C. Gautier, M. Geissel, D. Habs, R. Johnson, S. Karsch, A. Kemp, S. Letzring, M. Roth, U. Schramm, J. Schreiber, K. J. Witte, and J. C. Fernandez, *Phys. Plasmas* **12**, 056314 (2005).

<sup>17</sup>K. Flippo, B. Hegelich, M. Schmitt, C. Meserole, G. Fisher, D. Gautier, J. Cobble, R. Johnson, S. Letzring, J. Schreiber, M. Schollmeier, and J. Fernández, *J. Phys. (France)* **133**, 1117 (2006).

<sup>18</sup>A. Pukhov, *Phys. Rev. Lett.* **86**, 3562 (2001).

<sup>19</sup>P. Neumayer, B. Aurand, M. Basko, B. Ecker, P. Gibbon, D. C. Hochhaus, A. Karmakar, E. Kazakov, T. Kühl, C. Labaune, O. Rosmej, A. Tauschwitz, B. Zielbauer, and D. Zimmer, *Phys. Plasmas* **17**, 103103 (2010).

<sup>20</sup>C. Dorrer, I. A. Begishev, A. V. Okishev, and J. D. Zuegel, *Opt. Lett.* **32**, 2143 (2007).

<sup>21</sup>L. Waxer, T. K. D.N. Maywar, J. H. Kelly, R. M. B.E. Kruschwitz, S. J. Loucks, C. S. D. D. Meyerhofer, S. F. B. Morse, and J. Zuegel, *Opt. Photonics News* **16**, 30 (2005).

<sup>22</sup>C. Stoeckl, S.-W. Bahk, J. Bromage, V. Y. Glebov, O. V. Gotchev, P. A. Jaanimagi, D. D. Meyerhofer, P. Nilson, T. C. Sangster, M. Storm, S. Sublett, W. Theobald, and J. D. Zuegel, paper presented at 9th International Fast Ignition Workshop, Cambridge, MA.

<sup>23</sup>J. J. Thomson, *Proc. R. Soc. London* **89**, 1 (1913).

<sup>24</sup>K. Harres, M. Schollmeier, E. Brambrink, P. Audebert, A. Blazevic, K. Flippo, D. C. Gautier, M. Geissel, B. M. Hegelich, F. Nurnberg, J. Schreiber, H. Wahl, and M. Roth, *Rev. Sci. Instrum.* **79**, 093306 (2008).

<sup>25</sup>I. W. Choi, C. M. Kim, J. H. Sung, T. J. Yu, S. K. Lee, I. J. Kim, Y. Y. Jin, T. M. Jeong, N. Hafz, K. H. Pae, Y. C. Noh, D. K. Ko, A. Yogo, A. S. Pirozhkov, K. Ogura, S. Orimo, A. Sagisaka, M. Nishiuchi, I. Daito, Y. Oishi, Y. Iwashita, S. Nakamura, K. Nemoto, A. Noda, H. Daido, and J. Lee, *Rev. Sci. Instrum.* **80**, 053302 (2009).

<sup>26</sup>W. Mroz, P. Norek, A. Prokopiuk, P. Parys, M. Pfeifer, L. Laska, M. P. Stockli, D. Fry, and K. Kasuya, *Rev. Sci. Instrum.* **71**, 1417 (2000).

<sup>27</sup>C. G. Freeman, G. Fiksel, C. Stoeckl, N. Sinenian, M. J. Canfield, G. B. Graeper, A. T. Lombardo, C. R. Stillman, S. J. Padalino, C. Mileham, T. C. Sangster, and J. A. Frenje, *Rev. Sci. Instrum.* **82**, 6 (2011).

<sup>28</sup>P. M. Stafford, J. L. Horton, K. R. Hogstrom, P. M. DeLuca, Jr., and D. Holmlin, *Int. J. Rad. Appl. Instrum. D. Nucl. Tracks Radiat. Meas.* **14**, 373 (1988).

<sup>29</sup>R. Mishra, C. Orlando, L. Tommasino, S. Tonnarini, and R. Trevisi, *Radiat. Meas.* **40**, 325 (2005).

<sup>30</sup>M. Mori, M. Kando, A. S. Pirozhkov, Y. Hayashi, A. Yogo, N. Yoshimura, K. Ogura, M. Nishiuchi, A. Sagisaka, S. Orimo, M. Kado, A. Fukumi, Z. Li, S. Nakamura, A. Noda, and H. Daido, *Plasma Phys. Controlled Nucl. Fusion Res.* **1**, 042 (2006).



- <sup>31</sup>N. Sinenian, M. J. Rosenberg, M. Manuel, S. C. McDuffee, D. T. Casey, A. B. Zylstra, H. G. Rinderknecht, M. G. Johnson, F. H. Séguin, J. A. Frenje, C. K. Li, and R. D. Petrasso, *Rev. Sci. Instrum.* **82**, 103303 (2011).
- <sup>32</sup>F. H. Séguin, J. A. Frenje, C. K. Li, D. G. Hicks, S. Kurebayashi, J. R. Rygg, B. E. Schwartz, R. D. Petrasso, S. Roberts, J. M. Soures, D. D. Meyerhofer, T. C. Sangster, J. P. Knauer, C. Sorce, V. Y. Glebov, C. Stoeckl, T. W. Phillips, R. J. Leeper, K. Fletcher, and S. Padalino, *Rev. Sci. Instrum.* **74**, 975 (2003).
- <sup>33</sup>J. A. Frenje, C. K. Li, F. H. Séguin, D. G. Hicks, S. Kurebayashi, R. D. Petrasso, S. Roberts, V. Y. Glebov, D. D. Meyerhofer, T. C. Sangster, J. M. Soures, C. Stoeckl, C. Chiritiescu, G. J. Schmid, and R. A. Lerche, *Rev. Sci. Instrum.* **73**, 2597 (2002).
- <sup>34</sup>See <http://www.dextermag.com> for "Dexter Magnetic Technologies."
- <sup>35</sup>P. Mora, *AIP Conf. Proc.* **920**, 98 (2007).
- <sup>36</sup>A. Mančić, J. Fuchs, P. Antici, S. A. Gaillard, and P. Audebert, *Rev. Sci. Instrum.* **79**, 073301 (2008).